Daniell method for power spectral density estimation in atomic force microscopy

Aleksander Labuda

Articles you may be interested in

An ultra-low noise optical head for liquid environment atomic force microscopy
Rev. Sci. Instrum. **86**, 083705 (2015); 10.1063/1.4928497

Preamplifying cantilevers for dynamic atomic force microscopy
Appl. Phys. Lett. **94**, 103507 (2009); 10.1063/1.3093814

Atomic force microscopy cantilever dynamics in liquid in the presence of tip sample interaction
Appl. Phys. Lett. **93**, 253106 (2008); 10.1063/1.3050532

Hydrodynamic damping of tip oscillation in pulsed-force atomic force microscopy
Appl. Phys. Lett. **77**, 3462 (2000); 10.1063/1.1325395

Dynamic force microscopy by means of the phase-controlled oscillator method
J. Appl. Phys. **82**, 3641 (1997); 10.1063/1.365726
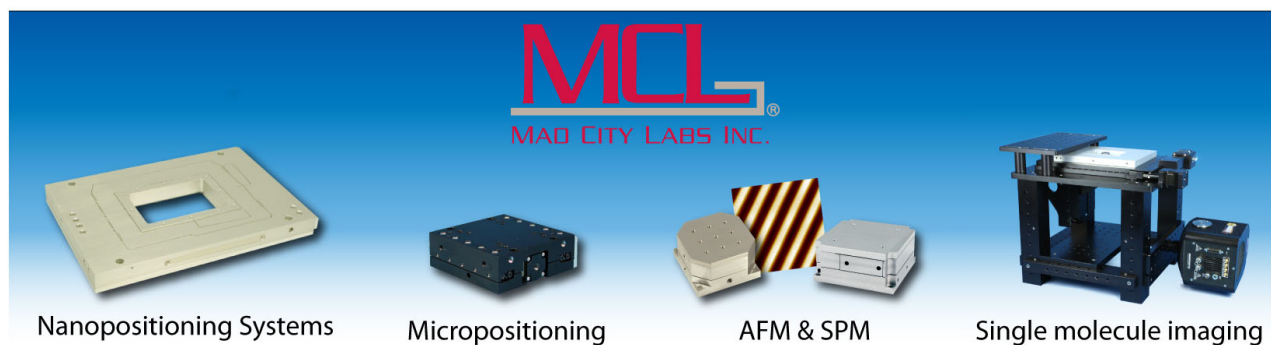
Daniell method for power spectral density estimation in atomic force microscopy

Aleksander Labuda

Asylum Research an Oxford Instruments Company, Santa Barbara, California 93117, USA

An alternative method for power spectral density (PSD) estimation—the Daniell method—is revisited and compared to the most prevalent method used in the field of atomic force microscopy for quantifying cantilever thermal motion—the Bartlett method. Both methods are shown to underestimate the Q factor of a simple harmonic oscillator (SHO) by a predictable, and therefore correctable, amount in the absence of spurious deterministic noise sources. However, the Bartlett method is much more prone to spectral leakage which can obscure the thermal spectrum in the presence of deterministic noise. By the significant reduction in spectral leakage, the Daniell method leads to a more accurate representation of the true PSD and enables clear identification and rejection of deterministic noise peaks. This benefit is especially valuable for the development of automated PSD fitting algorithms for robust and accurate estimation of SHO parameters from a thermal spectrum. © 2016 AIP Publishing LLC. [http://dx.doi.org/10.1063/1.4943292]

I. INTRODUCTION

Measuring the stiffness of cantilevers in the context of atomic force microscopy (AFM) has been a topic of primary importance in the field since its inception.[1–7] Many detection methods have been developed for accurately sensing cantilever deflections down to picometer precision.[8–13] However, the ultimate limit for accurately converting these deflections into nanoscale forces has been limited by difficulties in calibrating the cantilever stiffness. Furthermore, a variety of dynamic AFM imaging techniques,[14,15] where the cantilever is driven on resonance, rely on accurate calibration of the stiffness of the cantilever's first eigenmode. Also, a host of new multi-frequency nanomechanical mapping techniques[16–19] depend on accurate calibration of the stiffness of higher eigenmodes.[20,21]

Whereas a measure of cantilever stiffness is necessary for quantifying conservative tip-sample interactions, changes in damping of the cantilever relate to energy loss mechanisms. Dissipation measurements[22–27] provide complementary information about sample properties and atomic processes at the tip-sample junction. Such studies are of interest in environments ranging from vacuum, to air, water, and highly viscous fluids, all of which rely on accurate calibration of the cantilever damping before interaction with the sample.

Regardless of the measurement technique, any inaccuracy in calibrating the sensor—the cantilever—translates directly into a systematic error in interpreting the tip-sample conservative and dissipative interactions. Consequently, alongside these new technique developments, there have been studies dedicated to improving the estimation quality of cantilever stiffness and damping before tip-sample interaction occurs. The information about these parameters is contained in the power spectral density (PSD) of the cantilever's thermally driven stochastic motion.[28–36] Recent efforts have proved valuable in quantifying and correcting estimation biases[37–39] and

predicting the variance[40,41] in measurements of cantilever parameters from measured PSDs.

This paper focuses on the methodology used for estimating a PSD. An alternative method to the norm is presented and its performance is benchmarked on a typical AFM cantilever measurement with respect to determining its stiffness and damping. Although the simple harmonic oscillator (SHO) model is used as a point of discussion through most of this paper, the PSD estimation method presented here is especially useful for accurately estimating thermal spectrum of non-SHO stochastic oscillators in the presence of non-ideal noise sources, such as $1/f$ fluctuations and deterministic periodic noise.

Section II demonstrates the performance of two PSD estimation methods that will be discussed throughout the technical sections that follow. The comparison motivates the importance in choosing the appropriate PSD method for accurately quantifying cantilever thermal motion.

II. MOTIVATION: REVISITING PSD ESTIMATION METHODS

Since the dawn of information theory, many methods for the estimation of power spectral densities have been proposed. One of the first proposed approaches for estimating PSDs, anticipated by Einstein in 1941[42] and then proposed by Daniell in 1946,[43,44] amounts to performing a *single* PSD operation on a time series and then smoothing it to get a more precise estimate of the true PSD. Due to the limited computing resources throughout the 20th century, the popularity of this "Daniell method" for spectral estimation was short-lived and quickly superseded by other methods that remained prevalent until today. The simplest of these is the Bartlett method,[45] where the time series is split up into segments that are transformed into PSDs and then averaged together. Inevitably, splitting up a time series is accompanied by information loss and spectral distortion.
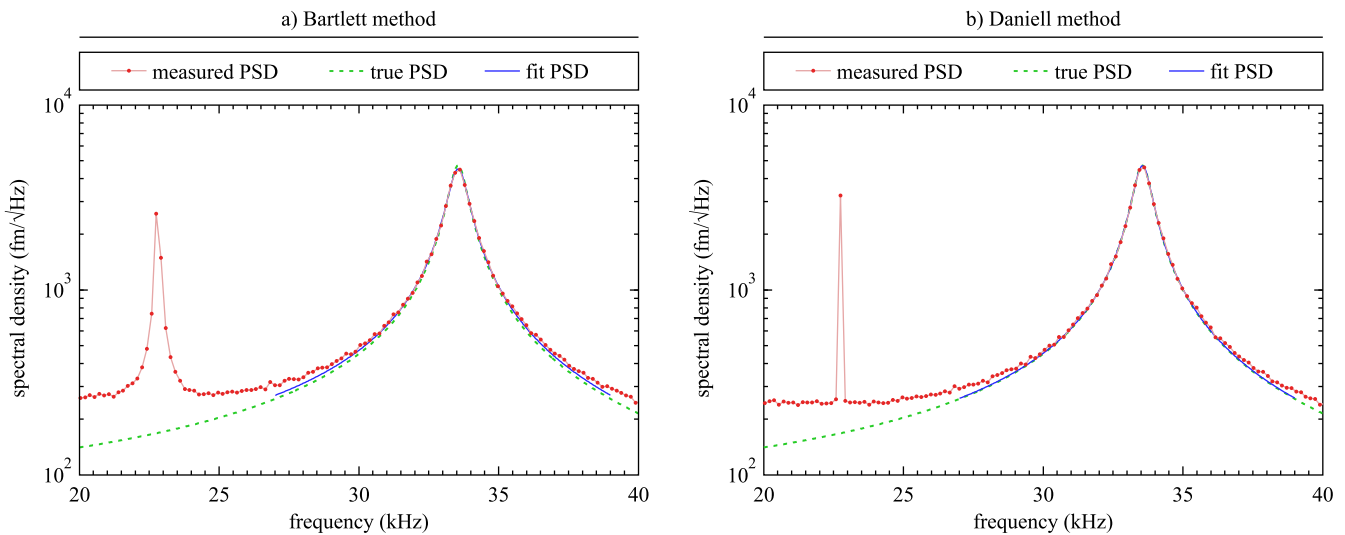
FIG. 1. A time series of cantilever deflection was acquired for 5 s with the LDV on a triangular silicon nitride cantilever (TR400-S, Olympus) with $Q = 52 \pm 1$. The PSD was computed using the (a) Bartlett method and the (b) Daniell method. Both methods with $\alpha = 6.0$. The peaks were fit with an SHO model and resulted in underestimated $Q = 47 \pm 1$ and $Q = 51 \pm 1$, respectively. Spectral leakage of the Bartlett method distorted the electronic noise peak around 22.7 kHz and broadened the SHO peak as can be seen from the inaccurate fit to the data. Note that the "fit PSD" data were plotted without the white noise component to illustrate deviations from the "true PSD." Movies of the time evolution of PSD averaging that simulate a live data stream are presented for both methods (enhanced online) ($M = 849$, $f_s = 5$ MHz, $N = 24\,999\,654$). (Multimedia view) [URL: http://dx.doi.org/10.1063/1.4943292.1] [URL: http://dx.doi.org/10.1063/1.4943292.2]

Despite these side effects, the Bartlett method remains a commonly used method for PSD estimation largely due to its simplicity.

Given the recent rise in computational power of desktop computers, it is worth revisiting the Daniell method. As a benchmark experiment, the power spectral density was computed from a times series of cantilever thermal motion. These thermal fluctuations were measured with a laser Doppler vibrometer (LDV) introduced into a Cypher AFM (Asylum Research) through a blueDrive™ optical system that was retrofit with broadband optics as in Ref. 46. Figure 1 (Multimedia view) compares the resulting PSDs computed using both the Daniell and the Bartlett methods. Due to the significant reduction in spectral leakage in this particular case, the Daniell method resulted in a more accurate estimate of the shape of the cantilever response: the error in Q factor determination dropped from 8% with the Bartlett method to 2% with the Daniell method. Also, the noise peak around 22.7 kHz can be correctly interpreted for the Daniell method as a deterministic periodic noise rather than some stochastic noise. The distinction between a deterministic and stochastic noise is elaborated upon in Appendix A; briefly, cyclical electronic noise is deterministic, while cantilever thermal motion is stochastic for typical AFM experiments.

In this article, the Daniell method is revisited and compared to the Bartlett method in terms of robustness, speed, accuracy, and precision in estimating PSDs in the context of studying the thermal spectrum of AFM cantilevers.

III. METHODOLOGY

The Bartlett and Daniell procedures for calculating PSD estimates are described in this section. The goal of both methods is to reduce the PSD variance by a factor of M, referred to as the "averaging factor."

Both methods start with a time series $x[n]$ acquired with a sampling frequency f_s. To facilitate the comparison of the Bartlett and Daniell methods in this context and to avoid certain mathematical idiosyncrasies, the time series $x[n]$ is truncated to impose the total number of samples N to be an even integer multiple of an odd averaging factor M. This ensures that M is odd, N is even, and N/M is an integer.

A. Bartlett method

For the Bartlett method, the time series is divided into M equal segments. The power spectral density $P[f]$ is computed as the squared magnitude of the Fourier transform for each segment, and all the results are averaged. Due to segmentation of the time series into M parts, the frequency resolution $f_\Delta = M/T$, where T is the duration of the time series.

The Bartlett method is graphically illustrated in Figure 2(a) and mathematically defined by

$$P_{\text{Bartlett}}[f] = \frac{2M}{f_\Delta N^2} \sum_{m=0}^{M-1} \left| \sum_{n=0}^{\frac{N}{M}-1} x\left[n + m\frac{N}{M}\right] \cdot e^{-2\pi i \frac{nM}{N} \frac{f}{f_\Delta}} \right|^2,$$

(1)

where i is the imaginary unit and f is the discrete frequency, defined as integer multiples of f_Δ up to $f_\Delta(N/M/2 - 1)$.

The DC offset ($f = 0$ Hz) and the Nyquist frequency ($f = f_\Delta N/M/2$) are both omitted in this particular implementation.

B. Daniell method

For the Daniell method, the squared magnitude of the Fourier transform of the *entire* time series is computed. Next, adjacent data points in the frequency domain are averaged
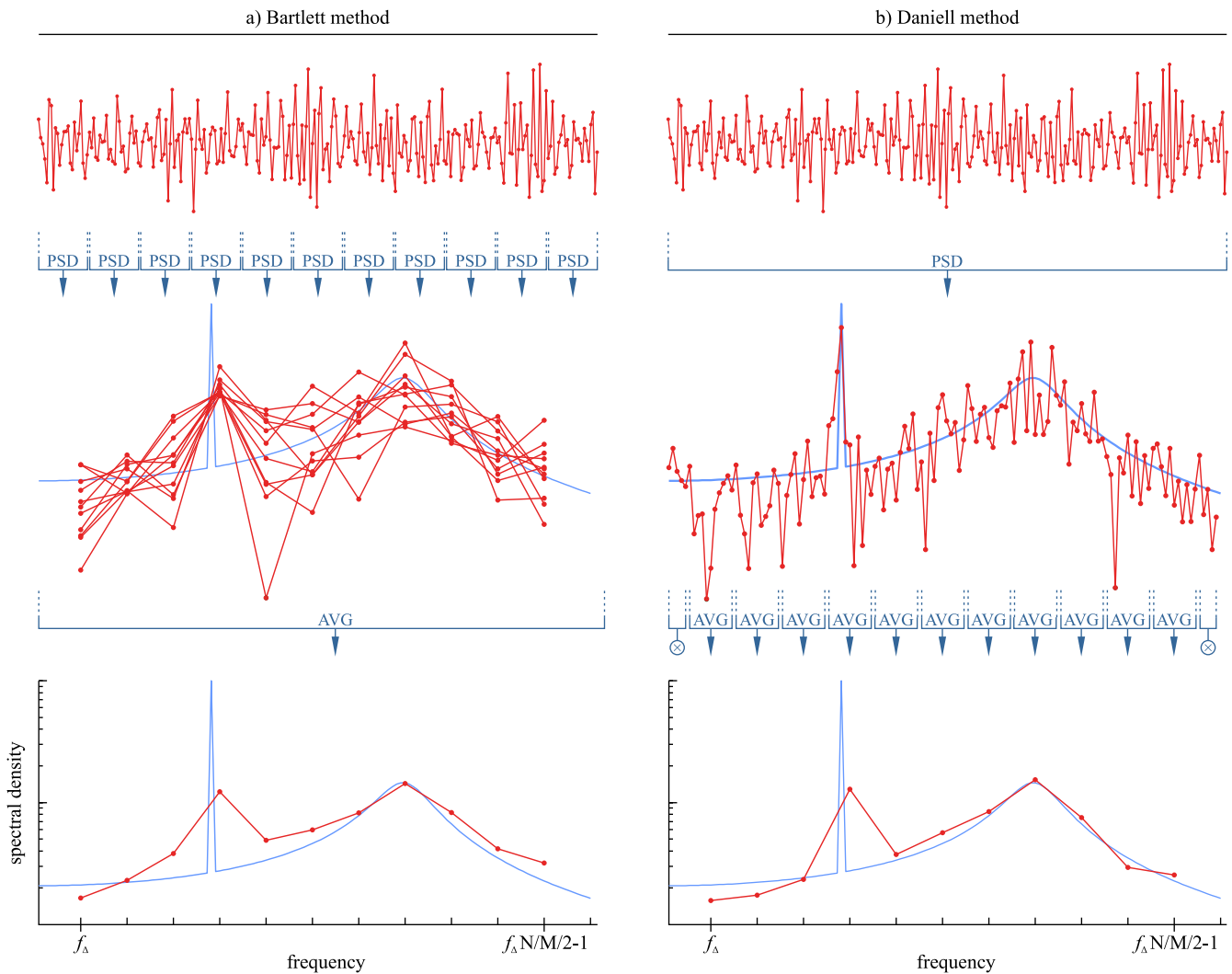
FIG. 2. The Bartlett and Daniell methods are illustrated graphically on simulated data to explain how a time series is converted into a power spectrum. The number of samples ($N = 264$) was chosen particularly low for illustrative purposes only. The Bartlett method divides a time series into segments, performs a PSD operation on each segment, and averages (AVG) the segments together to obtain a smooth PSD ($M = 11$ in this example). The Daniell method performs a single PSD on the whole time series, then averages adjacent frequency bins to obtain a smooth PSD (also $M = 11$). The underlying light blue curve represents the "true" PSD of the model used to simulate the data.

together in groups of M. Due to this averaging in the frequency domain, once again the frequency resolution $f_\Delta = M/T$.

Although the parameter M serves a different purpose in this context, the resulting frequency resolution f_Δ is identical in the Bartlett method. This explains why the same parameter M applies analogously to both methods and can be thought of as the "averaging factor" in either cases.

The Daniell method is graphically illustrated in Figure 2(b) and mathematically defined by

$$P_{\text{Daniell}}[f]$$

$$= \frac{2}{f_\Delta N^2} \sum_{m=0}^{M-1} \left| \sum_{n=0}^{N-1} x[n] \cdot e^{-2\pi i \frac{n}{N} \left(\frac{f}{f_\Delta/M} + m - \frac{M-1}{2} \right)} \right|^2. \quad (2)$$

As illustrated in Figure 2(b), the first and last $(M + 1)/2$ data points from the original PSD are discarded in this particular implementation. This is of no concern as the first few data points of a measured PSD are highly prone to drift, spectral leakage, and typically carry limited, if not misleading, information about the stochastic process being studied; the last

few data points are highly prone to aliasing. In that sense, the rejection of these data points is considered good riddance and is analogous to discarding the DC and Nyquist frequencies in the Bartlett method.

IV. ACCURACY AND BIAS

The accuracy of any PSD estimate suffers because the time window of the measurement is inevitably finite. This sets a lower bound on the frequency resolution of the estimated PSD to $1/T$. Importantly, additional spectral distortions can degrade the *effective* frequency resolution of the PSD even further, as discussed in this section.

A. Spectral distortion due to spectral leakage

The Fourier transform operation used to compute the PSD assumes that the finite time measurement is perfectly periodic with period T; that is, the last data point is considered contiguous to the first data point, leading to an infinite circular dataset.

The consequence is that any discontinuity between the last and first data points is assumed to be real measured information and affects the PSD estimate accordingly. For example, a perfectly sinusoidal noise that is truncated by a finite time window will appear discontinuous and result in spectral leakage (an exception to this occurs when exactly an integer number of cycles fits into the time window). Such spectral leakage led to the broadening of the 22.7 kHz peak in Figure 1(a).

A more subtle, yet important, consequence of spectral leakage is that any SHO peak in the estimated PSD will be broader than its true PSD counterpart. In Figure 1, spectral leakage broadened the shape of the thermal spectrum in the case of the Bartlett method. In order to correct for this broadening after the fact, Sader *et al.* have derived an expression for the effective quality factor Q_{eff} measured from a true Q subject to spectral leakage,[39]

$$Q_{\mathrm{eff}} = Q\left(1 - \frac{1}{2\alpha}\right), \qquad (3)$$

where

$$\alpha = \frac{\pi}{2Q}\frac{f_0}{f_\Delta}. \qquad (4)$$

The normalized α parameter measures the number of data points that make up the peak of a SHO. As an example, the very peak of the SHO in Figure 1 is defined by roughly 6 points and $\alpha \approx 6$. Eq. (3) is correct in the asymptotic limit $\alpha \gg 1$. Importantly, Eq. (3) requires the use of a rectangular window function, discussed later.

On the other hand, the spectral leakage in the Daniell method follows a different scaling law. Because spectral leakage occurs when the Fourier transform operation is performed, the Daniell method is subject to spectral leakage that is proportional to $1/T$, rather than the M/T observed in the Bartlett method. This factor of M facilitates attaining negligible levels of spectral leakage for a given application when using the Daniell method. For a given experiment, there will usually be some value of M that guarantees that the majority of the spectral leakage spans at most two frequency bins. (Regardless of the averaging factor M, a noise peak can always span up two frequency bins if it falls near the intersection of both bins.)

B. Spectral distortion due to frequency-averaging

The Daniell method is afflicted by a different form of spectral distortion caused by the fact that adjacent frequency bins are combined into a single bin during averaging. This distortion is represented graphically in Figure 3 on a noiseless theoretical SHO PSD. It can be understood from visual inspection that averaging a PSD section with negative curvature leads to an underestimation of the PSD value at the average frequency value. Conversely, a positive curvature leads to an overestimated PSD data point.

The functional form of the frequency-averaged SHO PSD is derived analytically in Appendix B. The consequence of frequency-averaging in the Daniell method is an underestimated Q factor of the SHO model that is fit to the data due to broadening of its peak. The effective Q factor can be approximated by
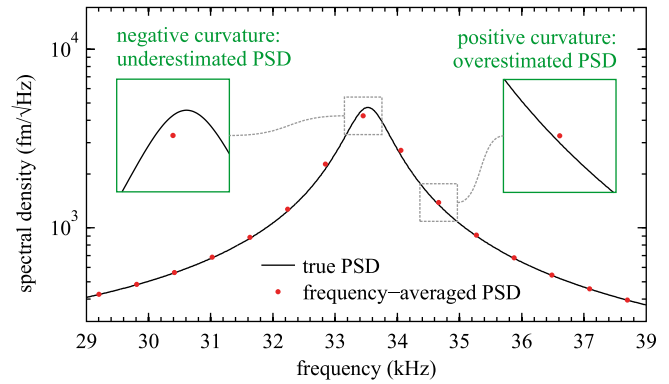

FIG. 3. The effect of binning data points in the frequency domain is illustrated here. The averaged data points may underestimate or overestimate the true PSD depending on the local curvature of the PSD.

$$Q_{\mathrm{eff}} = Q\left(1 - \frac{\pi^2}{12\alpha^2}\right), \qquad (5)$$

in the asymptotic limit $\alpha \gg 1$.

Importantly, the bias in the Q factor in the case of frequency-averaging scales as α^{-2}, which converges to the correct Q factor more quickly than the α^{-1} scaling caused by spectral leakage in the Bartlett method, seen in Eq. (3).

The bias in Q factor estimation of Eq. (5) can be inverted in order to recover the true Q in an experimental setting after measuring a biased Q_{eff}, as in

$$Q = Q_{\mathrm{eff}}\left(1 + \frac{\pi^2}{12\alpha^2} + \left(\frac{\pi^2}{12\alpha^2}\right)^2\right), \qquad (6)$$

where it was assumed that $Q_{\mathrm{eff}} \approx Q$, and the binomial approximation was carried out to second order. This inversion of Eq. (5) is accurate to within 0.1% for $\alpha > 3$.

V. PRECISION AND VARIANCE

The precision in the estimation of SHO parameters relates to the variance of the PSD data points. Both the Bartlett and Daniell methods perform linear averaging of data points that results in a calculable variance. The variance of each data point in the final PSD is equal to

$$Var\{P[f]\} = \frac{P[f]}{M}. \qquad (7)$$

This equation applies to stochastic noise and a rectangular window function. Other window functions, discussed later, may increase the variance of estimated PSD parameters due to loss of information.

Previously established analytical methodologies,[37,38,40] or stochastic simulations,[41,47] can be applied for studying how the variance of $P[f]$ relates to the variance of the SHO parameters.

VI. OPTIMIZATION

Much like the Bartlett method, the Daniell method can be optimized by choosing an averaging factor M that is most appropriate for the particular application, as well as tailoring the windowing function to minimize the effects of spectral
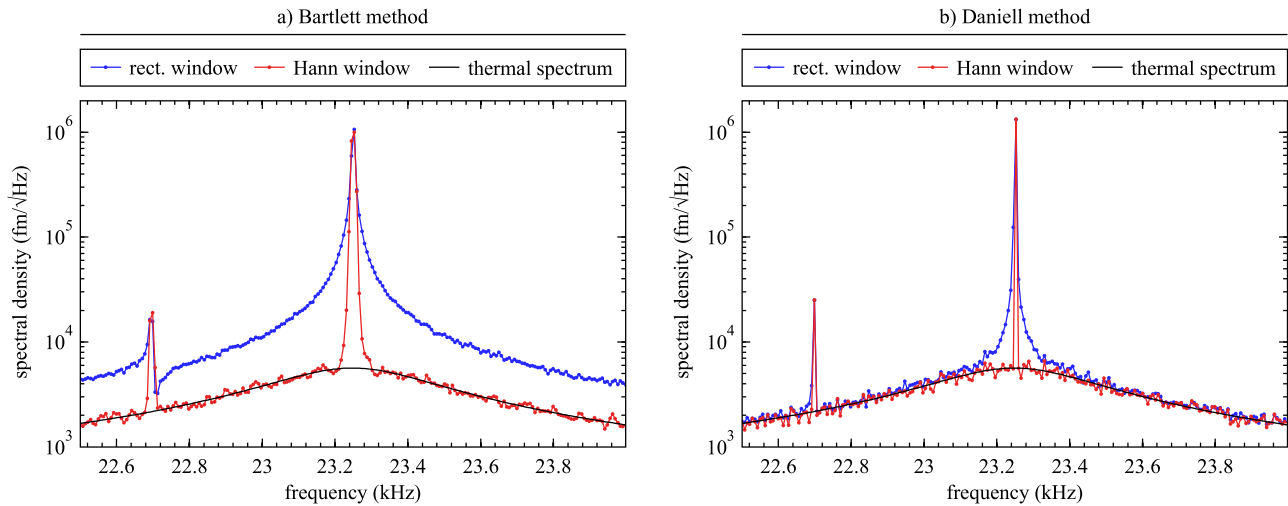
FIG. 4. The effects of spectral leakage are demonstrated on a PSD of a sinusoidally driven cantilever (TR800-L, Olympus) with an amplitude of 1 nm for the (a) Bartlett and (b) Daniell methods with rectangular and Hann window functions. The true cantilever thermal spectrum was acquired independently and also plotted for reference. The noise peak at 22.70 kHz originates from the LDV electronics ($M = 71$, $f_s = 5$ MHz, $N = 49\,999\,904$).

leakage. PSD averaging during live data acquisition requires additional considerations that are also discussed in this section.

A. Averaging factor M

The optimal averaging factor M for the Daniell method depends on the application. In the context of fitting an accurate SHO model, the threshold averaging number M_{SHO} can be defined by the desired level of accuracy in Q factor determination by

$$M_{SHO} < \sqrt{3}\epsilon \frac{T f_0}{Q}, \qquad (8)$$

where ϵ is the upper bound in relative Q estimation error, defined as $\epsilon = 1 - Q_{eff}/Q$.

However, there is a trade-off between minimizing the averaging factor for accuracy in the SHO parameters and the identification and isolation of deterministic noise peaks. In the presence of large amplitude deterministic noise peaks, larger values of M may be required to contain the spectral leakage to at most two frequency bins. As described in Sec. VI B, the required M to achieve this condition also strongly depends on the windowing function.

B. Windowing function

The Daniell method does not guarantee the prevention of spectral leakage, and it only scales the Fourier transform of the window function by a factor of $1/M$ (along the frequency axis) with respect to the Bartlett method. Depending on the amplitude of the deterministic noise peak relative to the stochastic background, a certain minimum value of M will be required to limit the bulk of spectral leakage into no more than two frequency bins.

Just as with the Bartlett method, the shape of spectral leakage can be tuned by the use of window functions. This directly impacts the choice of M required for limiting spectral leakage in any particular application. This idea is demonstrated

by example in Figure 4: the PSD of a sinusoidally driven cantilever was computed using the Bartlett and Daniel methods.

For a rectangular window function, the sinusoidal drive of the cantilever is shown to spectrally leak substantially for the Bartlett method, to the point of completely obscuring the underlying thermal spectrum. Recalculating the PSD with a Hann window function greatly reduces the spectral leakage.

Despite the large reduction in spectral leakage by the Daniell method, the rectangular window function still leads to a broadening of the sinusoidal drive peak. However, the use of a Hann window manages to contain the spectral leakage into a single frequency bin, making it easily distinguishable from the underlying thermal spectrum.

It is clear from Figure 4 that the use of window functions benefits both methods greatly. However, the Q factor correction for the Bartlett method (by inverting Eq. (3)) only applies to a rectangular window function,[39] which is very restrictive. Meanwhile, Q correction for the Daniell method (Eq. (6)) is *not* dependent on the window function because spectral leakage is negligible; only spectral distortion due to frequency-averaging requires correction.

The data in Figure 4 should be taken with a grain of salt. The usage of the Bartlett method does not always lead to spectral leakage: if the data series is timed precisely to contain an integer number of cycles of a deterministic noise source, then no spectral leakage occurs. In that sense, the data presented in Figure 4 represent only a possible outcome of an experiment. However, it is a fact that any window function for the Daniell method is exactly M times narrower (in the frequency domain) than its Bartlett counterpart and it sets the upper bound for spectral leakage in a PSD.

C. Live implementation

So far, the discussion has been based around calculating the PSD of a pre-recorded time series of duration T, and determining the optimal averaging factor M. The details of the discussion differ when considering a live stream of data.

When presenting live PSD averaging, the M factor would typically not be defined *a priori*. In that case, a frequency resolution f_Δ is defined before the acquisition by $f_\Delta = 1/T^*$, where T^* is the predetermined duration of each measured time segment. As more data segments are acquired with time, the averaging factor M increases. This rationale can be applied to both the Bartlett and Daniell methods, as presented by the movies in Figure 1 (Multimedia view). This will be referred to as the "preferred implementation" for live PSD averaging for both methods.

The advantage of the Daniell method is that both the variance and spectral leakage scale as M^{-1} for this preferred implementation. Therefore, spectral leakage can be made negligible by acquiring more data, as demonstrated in Figure 1. Meanwhile, the Bartlett spectral leakage remains fixed as more data are acquired; only the variance scales as M^{-1}. In other words, additional data do not result in a clearer distinction between deterministic and stochastic noise sources for the Bartlett method.

The disadvantage of the Daniell method is that it requires the entire time series acquisition to be continuous, such that hardware memory limits the maximum duration T. Also, performing a PSD calculation on an increasingly longer time series requires ever more computing power. Meanwhile, the Bartlett method allows interruptions between the M time segments, and the repeated PSD operation acts on time series of a predetermined duration T^*. Therefore, Bartlett averaging can go on forever if past time segments are being discarded.

For these reasons, the Bartlett method may be more practical for live PSD averaging in certain experimental settings. Nevertheless, as long as the entire time series is acquired continuously, it can be post-processed by the Daniell method to reap the benefits of reduced spectral leakage.

VII. RELATING EXPERIMENTAL TO PHYSICAL PARAMETERS

Although the physical parameters of interest for characterizing an AFM cantilever are its stiffness k and damping b, the parameters that are used in fitting the thermal spectrum are its resonance frequency f_0, quality factor Q, for practical reasons. In fact, the calibration method developed by Sader *et al.*[48–50] and implemented by Asylum Research as GetReal™ relies solely on a measurement of f_0 and Q to estimate the cantilever stiffness k relative to a set of reference cantilevers previously calibrated by interferometry. The advantage of this approach is that f_0 and Q can be measured on *any* AFM and do not require interferometry, yet they can be used to calculate the stiffness of the cantilever by Sader's semi-empirical theory.[48]

In this context, the errors in the experimental parameters (Q, f_0) can be related to the physical parameters of interest (k, b) by the following scaling laws:[48,49]

$$k \propto Q f_0^{1.3} \tag{9}$$

and

$$b \propto f_0^{0.3}. \tag{10}$$

Whereas f_0 can be measured quickly and accurately in ambient conditions, the Q factor is much more susceptible to bias and noise. This explains the emphasis that has been placed on estimation of Q so far.

VIII. BENCHMARK

First, the Bartlett and Daniell methods will be compared with regards to their performance in determining the true Q factor of a thermally driven cantilever. Then, an automated fitting algorithm that rejects deterministic noise peaks will be tested using both methods.

A. Q factor bias

A stochastic simulation based on methodology described previously[41,47] was used for comparing both methods. The cantilever from Figure 1 was used as a test case. A 5-s long time series of cantilever motion was simulated and PSDs were calculated for a wide range of averaging values M. Nonweighted least-squares fitting was used to fit an SHO model to the measured PSD data to obtain a Q factor estimate. This process was repeated 15 000 times to obtain very precise estimates of the average Q factor as a function of M. The results are presented in Figure 5.

As predicted, the accuracy of the Q factor estimation suffers for large M, and correspondingly low α, for both methods. The theory derived in Section IV is overlaid onto the data in Figure 5 and shows very good agreement. In other words, both the Bartlett and Daniell analytical predictions (Eqs. (3) and (5)) of Q factor estimation bias are very accurate down to α as low as 5. This level of predictability implies that the bias can be corrected after fitting the PSD, and the true Q factor of the cantilever can be recovered after spectral distortion occurs. Although the theory in Section IV was derived under the assumption that $\alpha \gg 1$ and $Q \gg 1$, these conditions are easily fulfilled in ambient environments by nearly all commercial AFM cantilevers.

The variance of each SHO fit parameter was also measured for the simulation in Figure 5. The results were the same for both methods because they are based on linear averaging of data points as described in Section V. It is the total
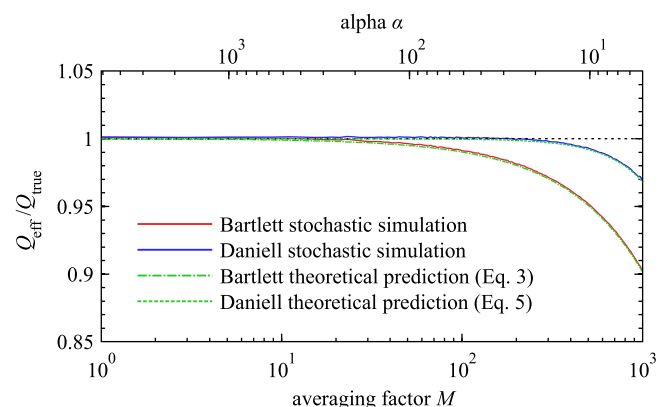

FIG. 5. The results from a stochastic simulation show deviations of the measured Q factor from the true Q factor as the averaging factor M is increased (or equivalently the alpha factor α is decreased, shown on the secondary x-axis). Both biases are predictable by analytical theory, also plotted. A rectangular window function was used.

measurement time T that ultimately determines the variance of SHO parameters. In this example, where $T = 5$ s, the normalized standard deviations $\sigma_Q = 2.5\%$, $\sigma_{f_0} = 0.02\%$, and $\sigma_{A_0} = 2.5\%$ for both methods.

The random errors σ_Q and σ_{f_0} convert to errors in stiffness $\sigma_k = 2.5\%$ and damping $\sigma_b = 0.01\%$ by the scaling laws presented in Section VII. Clearly, this low damping error σ_b is actually overshadowed by systematic calibration errors on the order of 1% that would have affected the interferometric calibration of the reference cantilevers. Nevertheless, the efforts in correcting the Q factor bias to well below 1% by the equations in Section IV are worthwhile for accurately estimating the stiffness in this context.

B. Case study: Automated noise filter performance

An algorithm for automated removal of deterministic noise peaks from a PSD is demonstrated in this section. The goal is to clean the PSD in order to more accurately fit the cantilever thermal spectrum. The algorithm is based on the simple idea that large and abrupt changes in the PSD relate to deterministic noise, while a thermal spectrum has a broad shape that changes smoothly across the PSD.

First, the thermal fluctuations of a cantilever were measured on a standard Cypher AFM, which is free of deterministic noise in the vicinity of the cantilever's resonance ($f_0 = 23.3$ kHz), to provide an accurate estimate of the Q factor. Then, the thermal motion was measured with the previously described LDV, and its PSD was computed with the Bartlett and Daniell methods. Both PSD's are corrupted by an electronic noise peak at 22.7 kHz, which was filtered by a noise filtering algorithm, as presented in Figure 6.

The noise filtering algorithm used here specifically calculates differences between adjacent PSD data points and rejects any data points that deviate from their neighbors by some threshold value (tuned to prevent false positives). Then, each noise-filtered PSD was fit with an SHO model, as shown in Figure 6. The Q factor fit to the Daniell PSD is accurate within random error of 1%, while the noise-filtered Bartlett PSD underestimates the Q factor by 13% in this particular case. The lowering of the fit Q factor is attributed to spectrally-leaked noise that was unsuccessfully filtered by the algorithm. The same algorithm was much more efficient at filtering the noise peak in the Daniell PSD whose power was concentrated in a single frequency bin.

Although it is possible to construct more sophisticated algorithms for removing deterministic noise peaks, it is clear by inspection of Figure 1 that removing such peaks is easier for PSD's estimated with the Daniell method. As shown in Figure 4(a), removing a spectrally leaked noise peak may be difficult when using the Bartlett method or even impossible if the rectangular window function is used.

It is important to note that acquiring a longer time series does not resolve the difficulty isolating a spectrally leaked deterministic noise peak from a thermal spectrum for the Bartlett method. The number of data points making up the spectrally leaked sine wave is determined by the shape of the window function (and number of cycles within the time series), and *not* the duration of the time series.
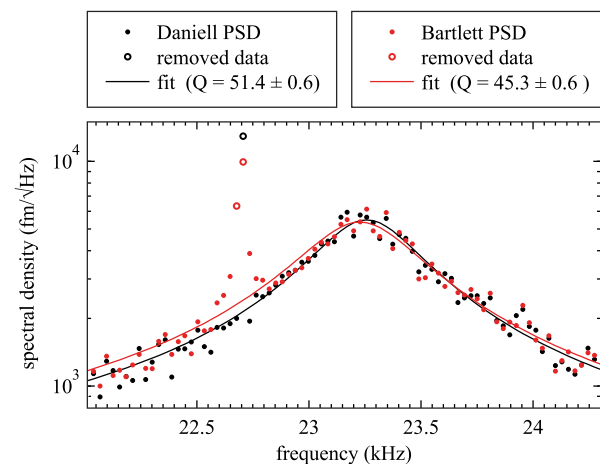

FIG. 6. The thermal spectrum of the cantilever from Figure 4 was computed with the Daniell and Bartlett methods. Then, a noise filtering algorithm was applied to both PSD's to remove the electronic noise peak at 22.7 kHz. The true $Q = 51.9 \pm 0.6$ was measured independently. A fit to the Bartlett PSD underestimated the true Q by 13% despite the removal of most of the deterministic noise peaks. The Daniell PSD with noise removal resulted in the correct Q factor within error ($\pm 1\%$) ($M = 29$, $f_s = 5$ MHz, $N = 4\,999\,948$).

IX. DISCUSSION

Both the Bartlett and Daniell methods have similar estimation variance and allow for accurate recovery of the Q factor (after correction) in cases where a clean thermal spectrum can be measured. However, the Bartlett method requires the use of a rectangular windowing function in order to correct for Q factor bias by solving Eq. (3). A rectangular window function can cause significant spectral leakage of deterministic noise peaks that may be difficult to isolate from the thermal spectrum. Spectral leakage may take a theoretically sharp peak and distort it into an SHO-like noise source in a measured PSD by the Bartlett method. This may render the noise peak and the SHO peak indistinguishable and prevent cantilever calibration, as reported by Sader *et al.* during the calibration of certain reference cantilevers whose resonance frequencies were close to those of electronic noise peaks.[48] Also, the presence of a deterministic noise peak may invalidate the calibration of a cantilever by an automated PSD fitting procedure applied by AFM software in the field.

A notable benefit of the Daniell methodology is that spectral leakage of deterministic noise peaks can be significantly reduced, and limited to spanning at most two frequency bins with the appropriate choice of averaging factor M and window function. In this case, deterministic noise peaks can be clearly identified and removed before fitting an SHO model to the PSD, thereby allowing robust and accurate calibration of the cantilever stiffness and damping. The removal of electronic noise peaks is especially useful for very high Q cantilevers,[51,52] such as in vacuum experiments, where the cantilever thermal noise can easily be mistaken for electronic noise and *vice versa*. Reducing the burden in distinguishing between stochastic and deterministic noise sources paves the way for accurate and robust automated PSD fitting software and AFM automation algorithms.

Furthermore, the large reduction in spectral distortion of the Daniell method carries important consequences for esti-

mating PSDs that deviate from the SHO model. The frequency dependence of damping,[4,22,53,54] $1/f$ multiplicative noise,[11,55] and other deviations from ideal SHO behaviour[4,56–59] require PSD estimation methods that have reduced bias at their root, as opposed to correcting for bias after-the-fact by assuming some model for the measured spectrum. In those types of cases, the fast reduction in bias by the α^{-2} scaling law of the Daniell method (see Eq. (5)) has a clear advantage because it may be impossible to correct for any biases if the true PSD functional form is unknown.

Fundamentally, the benefits of the Daniell method can be attributed to the fact that the PSD operation is performed on the entire time series. This preserves all the information when the PSD is being computed. On the other hand, the segmenting of the time series into M pieces by the Bartlett method results in information loss. Specifically, this may result in up to M times wider spectral leakage.

Similarly to other PSD estimation methods, the Daniell method can benefit from windowing to reduce the effects of spectral leakage, especially in situations with large deterministic noise peaks. In particular, a rectangular window function is *not* recommended for the Daniell method. A combination of the proper window function and optimal M factor depends on the dynamic range and nature of the signals being measured. For typical AFM scenarios, the use of a Tukey window that tapers only a small percentage of the time series may be optimal. Tapering only the very edge of the Tukey window may be sufficient to reduce spectral leakage to at most two frequency bins in most cases, while avoiding an increase in variance of SHO parameters due to information loss caused by windowing.

The disadvantages of the Daniell method are only technical in nature. The primary drawback is that it requires the storage of the entire time series. In contrast, the Bartlett method performs the Fourier transform on smaller time segments which can be discarded as the data are being acquired and the PSD's are being averaged. Another, yet less significant, drawback of the Daniell method is the additional time required to compute the Fourier transform of a single long time series versus several shorter ones. For large sample numbers N, both methods obey a scaling law of order $O(N) = N \log(N)$, but the Daniell method requires between $2\times$ and $6\times$ more computation time with respect to the Bartlett method.[63] To put this into perspective, the PSD calculations in Figure 1 took 0.7 s and 1.7 s for the Bartlett and Daniell methods, respectively.[63]

X. CONCLUSION

In conclusion, the Daniell method is an alternative PSD estimation method to the well-established Bartlett method that carries advantages in certain experimental settings, especially when the presence of deterministic noise peaks corrupts the measurement of a stochastic process. Although both methods result in the same parameter variances, and both allow straightforward correction of the Q factor estimation bias, deterministic noise peaks are much more difficult to isolate with the Bartlett method due to spectral leakage. This represents a burden on automated fitting algorithms, which can be alleviated by the use of the Daniell method.

Whereas both methods benefit from appropriate windowing of the time series, the Daniell method leads to $M\times$ less spectral leakage because the segmentation of the time series in M segments, which leads to information loss, is avoided.

Although the Bartlett method is less computationally intensive and requires less memory, the Daniell method has promising applications for experiments where spectral leakage needs to be minimized to avoid distorting the measured PSD of a stochastic process. Also, studies of stochastic oscillators that do not obey well established models (such as the simple harmonic oscillator model) can benefit from the significant reduction in spectral distortion offered by the Daniell method.

The methodology presented here for accurately measuring the thermal spectrum of simple harmonic oscillators in AFM can analogously benefit other fields, such as optical trapping,[60–62] that rely on power spectral density estimation for accurate instrument calibration.

APPENDIX A: DETERMINISTIC VS STOCHASTIC NOISE

The distinction between deterministic and stochastic noise depends on the context and the time scale of the experiment.

For example, cantilever thermal noise may look purely sinusoidal for durations of hundreds of milliseconds in cryogenic environments where the Q factors reach several tens of thousands. In this case, the PSD of the cantilever SHO may fall into a single frequency bin and be considered deterministic: the cantilever position and velocity at the beginning of the time series mostly determine the entire trajectory.

On the other hand, highly cyclical electronics noise may look stochastic when observed across days, as the phase may drift due to variations in temperature, for example.

Although somewhat arbitrary, a distinction between stochastic and deterministic noise may be drawn by comparing the coherence time of the noise source to the duration of the experiment. In the context of this paper, the duration of the experiment is the time series duration T, while the coherence time of a SHO is defined as $2Q/f_0$. According to this criterion, the thermal noise of cantilevers is highly stochastic in ambient conditions, while periodic electronic noise sources are typically highly deterministic.

APPENDIX B: QUANTIFYING Q BIAS FOR DANIELL METHOD

A SHO with stiffness k, mass m, and damping b has a transfer function with squared magnitude

$$|C|^2 = \frac{1}{[k - m\omega^2]^2 + [\omega b]^2}, \tag{B1}$$

with units of $\mathrm{m^2/N^2}$. The motion of this SHO is driven by stochastic thermal driving force

$$F(\omega) = 4k_B T b, \tag{B2}$$

with units of N^2/Hz, where k_B is the Boltzmann constant, and T is the temperature. The measureable PSD of this SHO is given by the product

$$P(\omega) = F(\omega) \times |C|^2, \tag{B3}$$

with resulting units of m^2/Hz, where $P(\omega)$ is the continuous PSD analog of the discrete PSD $P[f]$ described earlier.

Using the definition of the resonance frequency $\omega_0 = \sqrt{k/m}$ and $Q = k/\omega_0 b$, the above PSD can be rewritten in a more experimentally convenient form as

$$P(\omega) = \frac{4k_B T \omega_0^3}{kQ} \times \frac{1}{\left[\omega_0^2 - \omega^2\right]^2 + \left[\frac{\omega_0 \omega}{Q}\right]^2}. \tag{B4}$$

At high Q values, this distribution approaches a Lorentzian shape around the resonance, which warrants the following approximation:

$$P(\omega) = \frac{k_B T \omega_0}{kQ} \times \frac{1}{\left[\omega_0 - \omega\right]^2 + \left[\frac{\omega_0}{2Q}\right]^2}. \tag{B5}$$

Performing frequency-averaging by grouping adjacent frequency bins is analytically equivalent to convolving $P(\omega)$ with the uniform distribution

$$\mathcal{U}(\omega|\omega_R) = \begin{cases} 1/\omega_\Delta & \text{if } |\omega| < \omega_\Delta/2 \\ 0 & \text{if } |\omega| > \omega_\Delta/2 \end{cases}, \tag{B6}$$

where ω_Δ represents the frequency resolution of the final frequency-averaged PSD. This convolution

$$\begin{aligned} (P * \mathcal{U}) &= \int_{-\infty}^{\infty} P(\Omega)\, \mathcal{U}(\omega - \Omega)\, d\Omega \\ &= \frac{1}{\omega_R} \int_{\omega - \frac{\omega_\Delta}{2}}^{\omega + \frac{\omega_\Delta}{2}} P(\Omega)\, d\Omega \end{aligned} \tag{B7}$$

results in the Daniell PSD functional form

$$\begin{aligned} P_{\text{Daniell}}(\omega|\omega_\Delta) = \frac{2k_B T}{k\omega_\Delta} \times &\left[\tan^{-1}\left(\frac{2Q}{\omega_0}\left(\omega + \frac{\omega_\Delta}{2} - \omega_0\right)\right) \right. \\ &\left. - \tan^{-1}\left(\frac{2Q}{\omega_0}\left(\omega - \frac{\omega_\Delta}{2} - \omega_0\right)\right) \right]. \end{aligned} \tag{B8}$$

Evaluating the above expression at the resonance ($\omega = \omega_0$) simplifies to

$$P_{\text{Daniell}}(\omega_0|\omega_\Delta) = \frac{4k_B T}{k\omega_\Delta} \arctan\left(\frac{Q\omega_\Delta}{\omega_0}\right). \tag{B9}$$

This can be expressed in terms of the normalized α parameter by substituting

$$\omega_\Delta = \frac{\pi}{2Q}\frac{\omega_0}{\alpha}, \tag{B10}$$

and approximated by the Taylor expansion

$$\arctan(x) = x - x^3/3 + [\ldots] \tag{B11}$$

into

$$P_{\text{Daniell}}(\omega_0|\omega_\Delta) = \frac{4k_B T}{k\omega_0} Q\left[1 - \frac{1}{12}\left(\frac{\pi}{\alpha}\right)^2\right]. \tag{B12}$$

Therefore, the effective Q factor in the vicinity of the resonance peak becomes

$$Q_{\text{eff}} = Q\left[1 - \frac{1}{12}\left(\frac{\pi}{\alpha}\right)^2\right], \tag{B13}$$

as a good approximation for $\alpha \gg 1$.

[1] J. P. Cleveland, S. Manne, D. Bocek, and P. K. Hansma, Rev. Sci. Instrum. **64**, 403 (1993).
[2] C. T. Gibson, G. S. Watson, and S. Myhra, Nanotechnology **7**, 259 (1996).
[3] J. E. Sader, I. Larson, P. Mulvaney, and L. R. White, Rev. Sci. Instrum. **66**, 3789 (1995).
[4] J. E. Sader, J. Appl. Phys. **84**, 64 (1998).
[5] J. E. Sader, J. W. M. Chon, and P. Mulvaney, Rev. Sci. Instrum. **70**, 3967 (1999).
[6] J. L. Hutter and J. Bechhoefer, Rev. Sci. Instrum. **64**, 1868 (1993).
[7] N. A. Burnham, X. Chen, C. S. Hodges, G. A. Matei, E. J. Thoreson, C. J. Roberts, M. C. Davies, and S. J. B. Tendler, Nanotechnology **14**, 1 (2003).
[8] G. Meyer and N. M. Amer, Appl. Phys. Lett. **53**, 1045 (1988).
[9] Y. Martin, C. C. Williams, and H. K. Wickramasinghe, J. Appl. Phys. **61**, 4723 (1987).
[10] A. Labuda and P. H. Grütter, Rev. Sci. Instrum. **82**, 013704 (2011).
[11] A. B. Churnside, R. M. A. Sullan, D. M. Nguyen, S. O. Case, M. S. Bull, G. M. King, and T. T. Perkins, Nano Lett. **12**, 3557 (2012).
[12] B. W. Hoogenboom, P. L. T. M. Frederix, J. L. Yang, S. Martin, Y. Pellmont, M. Steinacher, S. Zäch, E. Langenbach, H.-J. Heimbeck, A. Engel, and H. J. Hug, Appl. Phys. Lett. **86**, 074101 (2005).
[13] D. Rugar, H. J. Mamin, and P. Guethner, Appl. Phys. Lett. **55**, 2588 (1989).
[14] R. García, Surf. Sci. Rep. **47**, 197 (2002).
[15] F. J. Giessibl, Rev. Mod. Phys. **75**, 949 (2003).
[16] R. Garcia and R. Proksch, Eur. Polym. J. **49**, 1897 (2013).
[17] A. Gannepalli, D. G. Yablon, A. H. Tsou, and R. Proksch, Nanotechnology **22**, 355705 (2011).
[18] T. R. Rodríguez and R. García, Appl. Phys. Lett. **84**, 449 (2004).
[19] R. Garcia and E. T. Herruzo, Nat. Nanotechnol. **7**, 217 (2012).
[20] D. Kiracofe and A. Raman, J. Appl. Phys. **107**, 033506 (2010).
[21] J. Lübbe, M. Temmen, P. Rahe, A. Kühnle, and M. Reichling, Beilstein J. Nanotechnol. **4**, 227 (2013).
[22] A. Labuda, K. Kobayashi, K. Suzuki, H. Yamada, and P. Grütter, Phys. Rev. Lett. **110**, 066102 (2013).
[23] A. Labuda, Y. Miyahara, L. Cockins, and P. Grütter, Phys. Rev. B **84**, 125433 (2011).
[24] W. Hofbauer, R. Ho, R. Hairulnizam, N. Gosvami, and S. O'Shea, Phys. Rev. B **80**, 134104 (2009).
[25] D. S. Wastl, A. J. Weymouth, and F. J. Giessibl, Phys. Rev. B **87**, 245415 (2013).
[26] K. Suzuki, K. Kobayashi, A. Labuda, K. Matsushige, and H. Yamada, Appl. Phys. Lett. **105**, 233105 (2014).
[27] R. Proksch and S. V. Kalinin, Nanotechnology **21**, 455705 (2010).
[28] H.-J. Butt and M. Jaschke, Nanotechnology **6**, 1 (1995).
[29] A. Gannepalli, A. Sebastian, J. Cleveland, and M. Salapaka, Appl. Phys. Lett. **87**, 111901 (2005).
[30] X. Xu and A. Raman, J. Appl. Phys. **102**, 034303 (2007).
[31] P. D. Ashby and C. M. Lieber, J. Am. Chem. Soc. **126**, 16973 (2004).
[32] O. H. Willemsen, L. Kuipers, K. O. van der Werf, B. G. de Grooth, and J. Greve, Langmuir **16**, 4339 (2000).
[33] G. Malegori and G. Ferrini, Nanotechnology **22**, 195702 (2011).
[34] F. Liu, S. de Beer, D. van den Ende, and F. Mugele, Phys. Rev. E **87**, 62406 (2013).
[35] L. Bellon, J. Appl. Phys. **104**, 104906 (2008).
[36] M. T. Clark, J. P. Cleveland, and M. R. Paul, Phys. Rev. E **81**, 1 (2010).
[37] S. F. Nørrelykke and H. Flyvbjerg, Rev. Sci. Instrum. **81**, 075103 (2010).
[38] J. E. Sader, B. D. Hughes, J. A. Sanelli, and E. J. Bieske, Rev. Sci. Instrum. **83**, 055106 (2012).
[39] J. E. Sader, J. Sanelli, B. D. Hughes, J. P. Monty, and E. J. Bieske, Rev. Sci. Instrum. **82**, 095104 (2011).
[40] J. E. Sader, M. Yousefi, and J. R. Friend, Rev. Sci. Instrum. **85**, 025104 (2014).
[41] A. Labuda, M. Lysy, W. Paul, Y. Miyahara, P. Grütter, R. Bennewitz, and M. Sutton, Phys. Rev. E **86**, 031104 (2012).
[42] P. Bloomfield, *Fourier Analysis of Time Series: An Introduction* (John Wiley & Sons, New York, 2000), p. 261.

[43]P. J. Daniell, "Discussion on the paper by M. S. Bartlett 'On the theoretical specification and sampling properties of autocorrelated time-series,'" Suppl. J. R. Stat. Soc. **8**(1), 88–90 (1946).

[44]M. S. Bartlett, Suppl. J. R. Stat. Soc. **8**, 27 (1946).

[45]M. S. Bartlett, Nature **161**, 686 (1948).

[46]A. Labuda and R. Proksch, Appl. Phys. Lett. **106**, 253103 (2015).

[47]A. Labuda, M. Lysy, and P. Grütter, Appl. Phys. Lett. **101**, 113105 (2012).

[48]J. E. Sader, J. A. Sanelli, B. D. Adamson, J. P. Monty, X. Wei, S. A. Crawford, J. R. Friend, I. Marusic, P. Mulvaney, and E. J. Bieske, Rev. Sci. Instrum. **83**, 103705 (2012).

[49]J. E. Sader and J. R. Friend, Rev. Sci. Instrum. **85**, 116101 (2014).

[50]J. E. Sader and J. R. Friend, Rev. Sci. Instrum. **86**, 056106 (2015).

[51]O. Kuter-Arnebeck, A. Labuda, S. Joshi, K. Das, and S. Vengallatore, J. Microelectromech. Syst. **23**, 592 (2014).

[52]J. Lübbe, L. Troger, S. Torbrugge, R. Bechstein, C. Richter, A. Kuhnle, and M. Reichling, Meas. Sci. Technol. **21**, 125501 (2010).

[53]P. Paolino and L. Bellon, Nanotechnology **20**, 405705 (2009).

[54]A. Labuda, K. Kobayashi, D. Kiracofe, K. Suzuki, P. H. Grütter, and H. Yamada, AIP Adv. **1**, 022136 (2011).

[55]A. Labuda, J. R. Bates, and P. H. Grütter, Nanotechnology **23**, 025503 (2012).

[56]C. P. Green and J. E. Sader, J. Appl. Phys. **98**, 114913 (2005).

[57]A. Labuda and P. Grütter, Langmuir **28**, 5319 (2012).

[58]T. Pirzer and T. Hugel, Rev. Sci. Instrum. **80**, 035110 (2009).

[59]A. Labuda, K. Kobayashi, Y. Miyahara, and P. Grütter, Rev. Sci. Instrum. **83**, 053703 (2012).

[60]S. F. Tolić-Nørrelykke, E. Schäffer, J. Howard, F. S. Pavone, F. Jülicher, and H. Flyvbjerg, Rev. Sci. Instrum. **77**, 103101 (2006).

[61]T. T. Perkins, Laser Photonics Rev. **3**, 203 (2009).

[62]K. Berg-Sørensen and H. Flyvbjerg, Rev. Sci. Instrum. **75**, 594 (2004).

[63]The $N \log(N)$ scaling law and the increase in computation time for the Daniell method were tested in Matlab on an intel® Core™ i7 processor with averaging factor M up to 10^5. The computations times for the data in Figure 1 were performed on the same computer.